Haemolytic actinoporins interact with carbohydrates using their lipid-binding module

Tanaka, Koji
1Department of Chemistry and Biotechnology, The University of Tokyo

Caaveiro, Jose M. M.
Department of Bioengineering, School of Engineering, The University of Tokyo

Morante, Koldo
Department of Bioengineering, School of Engineering, The University of Tokyo

Tsumoto, Kouhei
Department of Chemistry and Biotechnology, The University of Tokyo | Department of Bioengineering, School of Engineering, The University of Tokyo | The Institute of Medical Science, The University of Tokyo

出版情報：Philosophical transactions of the Royal Society of London. Series B, Biological sciences, 2017-06-19. Royal Society of London
バージョン：
権利関係：

Hemolytic actinoporins interact with carbohydrates using their lipid-binding module.

Koji Tanaka[1], Jose M.M. Caaveiro[2,*], Koldo Morante[2], and Kouhei Tsumoto[1,2,3,*]

[1]Department of Chemistry and Biotechnology, School of Engineering, The University of Tokyo, Bunkyo-ku, Tokyo 113-8656, Japan, [2]Department of Bioengineering, School of Engineering, The University of Tokyo, Bunkyo-ku, Tokyo, 113-8656, Japan, [3]The Institute of Medical Science, The University of Tokyo, Minato-ku, Tokyo, 108-8639, Japan.

Corresponding author: JMMC, Email jose@protein.t.u-tokyo.ac.jp

Corresponding author: KT, Email tsumoto@bioeng.t.u-tokyo.ac.jp

Keywords: Pore-forming protein; biomolecular recognition; lipid-protein interaction; carbohydrate-protein interaction; X-ray crystallography; sea anemone toxin.

Footnote.

Current address for JMMC: Graduate School of Pharmaceutical Sciences, Kyushu University, 3-1-1 Maidashi, Higashi-Ku, Fukuoka, 812-8582, Japan.

ABSTRACT

Pore-forming toxins (PFTs) are proteins endowed with metamorphic properties that enable them to stably fold in water solutions as well as in cellular membranes. PFTs produce lytic pores on the plasma membranes of target cells conducive to lesions, playing key roles in the defensive and offensive molecular systems of living organisms. Actinoporins are a family of potent hemolytic toxins produced by sea anemones vigorously studied as a paradigm of alpha-helical PFTs, in the context of lipid-protein interactions, and in connection with nanopore technologies. We have recently reported that fragaceatoxin C (FraC), an actinoporin, engages biological membranes with a large adhesive motif allowing the simultaneous attachment of up to four lipid molecules prior to pore formation. Since actinoporins also interact with carbohydrates, we sought to understand the molecular and energetic basis of glycan recognition by FraC. By employing structural and biophysical methodologies, we show that FraC engages glycans with low affinity using its lipid-binding module. Contrary to other PFT requiring separate domains for glycan and lipid recognition, the small single-domain actinoporins economize resources by achieving dual recognition with a single binding module. This mechanism could enhance the recruitment of actinoporins to the surface of target tissues in their marine environment.

INTRODUCTION

Pore-forming toxins (PFTs) are water-soluble proteins that form transmembrane oligomeric pores on cellular membranes leading to cell damage [1-3]. PFTs comprise a heterogeneous family of proteins of various molecular sizes and number of domains, exhibiting a rich collection of target membranes and cell receptors, oligomerization states, and mechanisms of action. For example, human perforin and the complement membrane attack complex play a key role in the immune system [4, 5], whereas bacterial PFTs are potent virulence factors [1, 6].

To effectively attack their targets, PFTs recognize specific receptors on the cell surface such as lipids, carbohydrates, and proteins. In addition to lipids, with which PFTs must interact before, during, and after pore formation, some PFTs engage with secondary receptors on the membrane surface increasing their effective concentration and thus facilitating their oligomerization and assembly. For example, cholesterol-dependent bacterial cytolysins such as pneumolysin from *Streptococcus pneumoniae* [7], streptolysin O from *Streptococcus pyogenes* [7], and lectinolysin *from Streptococcus mitis* [8, 9], recognize glycans present on the membrane of target cells in addition to cholesterol [10]. *Vibrio cholerae* cytolysin (VCC) binds to glycans and lipids [11, 12], and the translocation apparatus of the cholera toxin specifically recognizes the sugar moiety of

ganglioside GM1 with high affinity [13]. Another PFT, aerolysin, is recruited to the cell membrane by the N-glycans of membrane associated proteins, and by the glycan region of GPI-anchored proteins [14]. The structure of several of these glycan-binding sites has been determined for some PFTs, showing that these toxins utilize discrete domains to recognize their carbohydrate receptors [15, 16].

Actinoporins are a group of small (~ 20 kDa) and singe-domain alpha-helical PFTs secreted by sea anemones lethal to crustaceans, mollusks and fishes [17]. Actinoporins achieve their target specificity by utilizing the lipid sphingomyelin (SM) as both a binding receptor [18] and an assembly co-factor [19]. The lytic activity of actinorins also depends on the physicochemical properties of the membrane such as lipid phases [20-22]. The most studied actinoporins are equinatoxin II [23], sticholysin II [24], and fragaceatoxin C (FraC) [25]. The mechanism of lipid-recognition and pore formation of FraC and other actinoporins has been recently described from both structural and energetic points of view [19, 26-28] (Figure 1), although some controversy remains about the nature of the assembled pore [29]. In addition, the structural features of the pores formed by actinoporins have potential biotechnological applications for the analysis of double- and single-stranded nucleic acids using nanopore technologies [30].

Interestingly, previous studies have consistently shown that actinoporins experience a substantial delay in their elution profile in size-exclusion chromatography columns due to specific interactions with the resin [31-33], which is largely composed of polymers of carbohydrate. However, the putative binding site for carbohydrates or their effect on the function and structure of actinoporins are still unknown.

We hypothesized that single-domain actinoporins may recognize lipids and carbohydrates by a mechanism different from that of multi-domain PFTs. Herein we have investigated the ability of FraC to interact with carbohydrates from structural, functional and energetic viewpoints. We characterized the binding site of a sulfated monosaccharide at high resolution by X-ray crystallography. Surprisingly, the carbohydrate pocket overlaps with the lipid-binding module of actinoporins. Our study reveals a novel recognition mechanism by an ancient PFT that could enhance the activity of actinoporins in their natural coastal habitats.

MATERIALS AND METHODS

Materials.

Sphingomyelin (SM) from porcine brain, 1,2-dioleoyl-sn-glycero-3-phosphocholine (DOPC)

and cholesterol were purchased from Avanti Polar Lipids (Alabaster, AL, USA). Glucose, galactose, mannose, fructose, N-acetyl glucosamine (GlcNAc), N-acetyl glucosamine 6-sulfate sodium salt (GlcNAc(6S)), raffinose, and maltopentaose were obtained from Sigma-Aldrich (St Louis, MO, USA). Sucrose and occasionally glucose was from Merck. Chondroitin sulfate C sodium salt was obtained from Nacalai tesque (Kyoto, Japan). Defibrinated horse blood was purchased from Nippon Biotest Laboratories (Tokyo, Japan). Defibrinated sheep blood was from Pronadisa. Recombinant endoglycoceramidase II (EGCase II) with Activator II was obtained from TAKARA Bio (Siga, Japan). Biotin-hydrazide was purchased from Dojindo Laboratories (Kumamoto, Japan). Phosphocholine (POC) chloride sodium salt hydrate was obtained from Tokyo Chemical Industry (Tokyo, Japan). Reagents for the crystallization of proteins were purchased from Hampton Research (Aliso Viejo, CA, USA). Other chemicals were from Wako (Tokyo, Japan).

Protein expression and purification.

FraC and muteins were expressed and purified as described previously [31], with minor modifications. Briefly, FraC was expressed in *Escherichia coli* BL21 (DE3) cells grown at 37 °C.

FraC was purified from the cell lysate with a Resource S cationic exchange column (GE Healthcare, Piscataway, NJ, USA) equilibrated with buffer A (50 mM Tris HCl, pH 7.4). The protein was eluted with increasing concentrations of NaCl in buffer B (50 mM Tris HCl, and 1 M NaCl, pH 7.4). The protein fractions were pooled and subjected to size exclusion chromatography (SEC) in a HiLoad 16/60 Superdex 75 pg column (GE Healthcare) equilibrated with SEC buffer (50 mM Tris HCl, 200 mM NaCl, pH 7.4).

Hemolysis of deglycosylated red blood cells (RBC).

Defibrinated horse blood was washed in 20 mM HEPES, 150 mM NaCl (pH 7.4). Washed RBC (1.8 ml at OD_{600} of 1.0, corresponding to approximately 1.2×10^8 cells) were incubated with EGCase II [34] (50 mU) at 37 °C overnight. RBC were then washed in 20 mM HEPES, 150 mM NaCl (pH 7.4). As a control, RBC were incubated without EGCase II. Aliquots of RBC treated with EGCase II or control RBC (260 µl, OD = 0.65) were incubated with FraC (19.5 nM) for 10 minutes followed by centrifugation at 3,000 × *g* for 1 min. The hemolysis was monitored by the absorbance of hemoglobin released to the supernatant at a wavelength of 412 nm.

Hemolytic assays.

The time course of hemolysis was measured in a V-660 Spectrophotometer (Jasco, Japan) at 600 nm. Hemolytic activity was monitored by adding FraC to a suspension of horse RBC at an initial OD_{600} of ~ 0.5, in a total volume of 1 ml at room temperature. Protein were added at final concentration 25 nM to a solution containing buffer supplemented with monosaccharides or PEG 200 at a concentration of 400 mM. High concentration of monosaccharides and PEG 200 produced no deleterious effects on the stability of RBC during the time course of the experiments as judged from OD_{600}. When the effect of the number of units in the saccharide was examined, hemolysis of sheep RBC was carried out in the presence of glucose, sucrose, raffinose, or maltopentaose at 37.5 mM in a PowerWaveTM XS microplate reader (Biotek, VT, USA) at 700 nm and 25º C with constant shaking and FraC at a final concentration of 2 nM.

The effect of the concentration of saccharide on hemolysis was determined by twofold serial dilutions of FraC in a 96-well plate with buffer supplemented with monosaccharides or PEG 200 in a cell of 200 µl. After an incubation period of 1 hour at room temperature, samples were centrifuged at 6,000 × *g* for 1 min. The absorbance of hemoglobin released to supernatant was monitored in a PHERAstar (BMG LABTECH, Ortenberg, Germany) at a wavelength of 412 nm.

Micro-array glycan screening.

FraC containing the additional residue Cys180 at the C-terminus was labeled using the fluorophore molecule Alexa Fluor 488 C_5-maleimide (Thermo Fisher Scientific, MA, USA). The labeled protein was separated from unreacted dye in a NAP-5 column (GE Healthcare). The labeling efficiency was calculated to be approximately 100% from the ratio of absorbance at 495 nm and 280 nm. FraC retained its full hemolytic activity after labeling and lyophilization. Such labeled FraC was first lyophilized, subsequently disolved in the appropriate volume and analyzed at the Consortium for Functional Glycomics (CFG) using a mammalian printed array (Ver 5.2) containing 609 different glycans [35]. Labeled FraC was screened at 2, 20 and 200 μg/ml. The results obtained from the screen are freely available on the public repository at the CFG web site (Request ID: 2971).

Surface plasmon resonance (SPR).

Chondroitin sulfate C (2 mg/ml) was oxidized using 2 mM sodium periodate in 20 mM sodium acetate (pH 5.5), and covalently attached to biotin using 10 μM Biotin-hydrazide in 100 mM

MES (pH 6.5) at room temperature. The biotinylated molecule was reduced using 100 mM sodium cyanoborohydride in 100 mM MES, pH 7.0. The biotinylated carbohydrate was subsequently immobilized to a Series S Sensor Chip SA on a Biacore T200 instrument (GE Healthcare) equilibrated with HBS-P buffer (10 mM HEPES, 150 mM NaCl, 0.005% Surfactant P20, pH 7.4) at 25 °C. Twofold serial dilutions of FraC were injected over immobilized chondroitin sulfate C for 60 s, and the dissociation was followed for an additional 600 s.

Crystal structure of FraC and GlcNAc(6S) complex.

A solution of microcrystals was first prepared like that described for unbound FraC [19]. Large rod-shaped single crystals of the complex of FraC and GlcNAc(6S) were obtained after mixing 1 µl of protein at 9 mg ml^{-1} in 10 mM Tris HCl and 50 mM GlcNAc(6S) (pH 7.4), 0.2 µl solution of micro-seeds, and 1 µl of crystallization solution composed of 19% PEG 3,350, 200 mM ammonium chloride and 100 mM Bis-Tris (pH 6.3). Suitable crystals appeared after one month at 20 °C. Crystals of an approximate size of 0.2 × 0.03 × 0.03 mm^3 were transferred to a solution of mother liquor supplemented with 20% glycerol and subsequently frozen in liquid nitrogen. Data collection was carried out at beamline AR-NW12A of the Photon Factory (Tsukuba, Japan) under

cryogenic conditions (100 K). The structure of the FraC was determined by the molecular replacement method using the coordinates of FraC (PDB entry code 3VWI) with the program PHASER [36]. The initial model was refined using the programs REFMAC5 [37] and COOT [38]. The quality of the final model was assessed using the programs COOT and PROCHECK [39]. Data collection and refinement statistics are shown in Table 1.

Affinity SEC chromatoghraphy.

A Superdex 200 10/300 GL column (GE Healthcare) was calibrated with Blue dextran 2000, acetone, and marker proteins (aprotinin, ribonuclease A, carbonic anhydrase, ovalbumin, conalbumin, aldolase and ferritin) from a Gel Filtration Calibration Kit (GE Healthcare). The void volume (V_0) and the column volume (V_{total}) were determined to be 7.6 ml and 21.2 ml, respectively. The elution profile of FraC (230 µg) was examined in the presence of SEC buffer supplemented with increasing concentrations of phosphocholine (POC) at 0, 2.5, 5, 10, 20, 40 and 80 mM. Assuming that a competition between the matrix of the column and POC for FraC is occurring, the relationship between the elution volume of the protein and the concentration of POC is the following [40]:

$$1 / (V - V_{non}) = (A / K_{POC}) \times [\text{POC}] + A \quad (1)$$

where, V is the elution volume for the protein, V_{non} is the elution volume for the protein in the absence of interaction with the gel matrix, [POC] is the concentration of ligand in solution, the constant K_{POC} is defined for binding the protein to POC, and the constant A is a factor pertaining to the interaction between the protein and column matrix.

RESULTS

Hemolytic activity.

Consistent with previous studies [19, 31], we showed here that actinoporins experience a large delay in the SEC elution profile with chromatographic columns composed of carbohydrates (Figure 2a). Because carbohydrates act as a weak receptor in the SEC column, we extrapolated that glycans present on biomembranes and tissues could play some role in the activity of FraC, possibly working as weak secondary receptors. To test this hypothesis we first monitored the hemolysis of RBCs treated with an endoglycoceramidase (EGCase II), which cleaves the linkage between the glycans and the ceramide regions of glycosphingolipids. Other glycosylation linkages in proteins or in other lipids are no affected by EGCase II [34]. Although the fraction of

glycolipids with respect to the total lipidome of the RBC is relatively small, as a result of the treatment with EGCase II the RBC turned less susceptible to the hemolytic activity of FraC with respect to untreated cells. This observation suggested that the presence of glycans on the cell membrane enhance the potency of the toxin in a moderate fashion (Figure 2b). Ceramides, the lipid product of the enzymatic reaction of EGCase II, have been shown to inhibit the activity of actinoporins in liposomes with little (5%) of no cholesterol present [41]. Although the effect of ceramides in the activity of actinoporins have not been studied in RBC yet, that study suggests an additional mechanism explaining the inhibition of hemolysis in Figure 2b.

To gain further insight, we tested the idea that monosaccharides could inhibit the hemolytic activity of FraC, since these small monosaccharides could compete with the glycans on the surface of RBC for the toxin without blocking the pore [42]. The extent of the inhibition was comparable among the few hexoses examined (glucose, galactose, mannose and fructose) (Figure 2c). In contrast, the monosaccharide GlcNAc had a greater inhibitory potency than that of the other hexoses, suggesting some degree of specificity. PEG200, a small molecule of similar molecular weight to that of the monosaccharides, produced the lowest inhibitory effect. The extent of the inhibition increased with the concentration of the hexose in a non-linear fashion,

exhibiting midpoints at high concentration of monosaccharide or PEG200. The inhibitory effect is also observed in the kinetic profiles, and when exposing the RBC to saccharides composed of progressively more hexose rings (Figure S1). This latter observation suggests an avidity effect, although the inhibition caused by the large oligosaccharides is likely influenced also by an osmotic protection effect, as reported earlier [43, 44]. Since GlcNAc is also slightly larger than other monosaccharides, the presumably greater osmotic protective effect of this monosaccharide may also play some role in the differences reported in Figure 2C and Figure S1a.

Because of the arguably low affinity of these sugars for the toxin, it was deemed necessary to examine other carbohydrates in order to find molecules with higher affinity for FraC. This search would be followed by a more direct characterization of the interaction between carbohydrates and FraC employing high-resolution structural and biophysical techniques.

Micro-array screening.

To elucidate the preference of FraC for certain carbohydrates, a comprehensive screen using a glycan array composed of 609 different mammalian glycans was performed. The screen was carried out with FraC labeled at the C-terminus with the fluorescent dye Alexa Fluor 488 attached

to an additional Cys residue appended at the C-terminus. The result of the screen failed to find a highly specific sugar, but instead it showed binding activity for a large subset of glycans (public data can be retrieved as indicated in the materials and methods section). Notably, sulfated glycans appeared most frequently among the highest-ranked glycans (Figure 3a).

These data suggested that FraC possesses the ability to engage with to a broad range of glycans, particularly with glycans modified with a sulfate group. Sulfated sugars are major components of glycosaminoglycans (GAGs), a class of carbohydrates rich in amino-sugars like GlcNAc. The stronger inhibitory potency of GlcNAc and the outcome of the experiment with the glycan micro-array suggested that GAGs are possibly low-affinity targets for FraC, at least *in vitro*. Because of the low binding affinity of small saccharides, we employed chondroitin sulfate C (a polysaccharide composed of alternating units of GlcNAc(6S) and glucuronic acid) as a representative member of this family of GAGs to quantify its binding affinity to FraC by SPR (Fig. 3b, c). Binding of FraC to chondroitin sulfate C immobilized on the sensor chip was monitored at various concentrations of toxin. The sensorgram displayed a classical box-shape [45], giving rise to a weak dissociation constant K_D = 23.6 µM, and a fast dissociation rate (k_{off} = 1.0 s^{-1}). The association rate was too fast to be reliable determined. The fast dissociation rate, and

the presence of negative charges in the polysaccharide and a positively charged surface in the lipid-binding region of FraC (Figure S2) [19], suggested an important role of the electrostatic forces in binding.

Structural basis of interaction between FraC and GlcNAc(6S).

The high resolution crystal structure of the complex of FraC with the sulfated monosaccharide GlcNAc(6S) was determined at 1.55 Å resolution (Table 1). Since the protein was crystallized from microcrystal seeds prepared like for the unbound protein (PDB entry code 3VWI), the crystals yielded the same space group and very similar cell-unit dimensions. In this particular three-dimensional arrangement, half of the protein chains are unavailable to engage the sugar because key binding residues are involved in crystal packing contacts, and therefore cannot interact with the monosaccharide.

The overall conformation of FraC was essentially identical to that of the unbound protein (RMSD = 0.19 ± 0.08 Å), or the lipid-bound species (PDB entry code 4TSQ; RMSD = 0.37 ± 0.04 Å) [19]. Interestingly, the binding site of GlcNAc(6S) overlaps with that of the fourth lipid (L4) described in the lipid-bound structure [19] (Figure 4a, b). The position of all atoms of the

monosaccharide in the crystal was unambiguously determined from the excellent features of the electron density maps (Figure 4c). Close investigation of the GlcNAc(6S)-binding site reveals several hydrogen bonds between oxygens of the sulfate group and the hexose ring of the sugar, with residues Arg53 and Gln130 of the protein (Figure 4c, d). The hydroxyl groups of aromatic residues Tyr51 and Tyr138 are members of hydrogen bond networks with the monosaccharide *via* interfacial water molecules. Notably, Arg53 and Tyr138 also formed hydrogen bonds with the phosphate oxygens of lipid L4 in the crystal structure with lipid bound [19] further demonstrating the overlap between the binding interfaces of lipid and carbohydrate (Figure 4e).

Several residues involved in both binding GlcNAc(6S) and lipids underwent conformational changes in their side-chains with respect to each other. These changes are clearly observed in residues Arg53, Glu130 and Gln134 (Figure 4f). Changes restricted to the relative position of residues belonging to the aromatic cluster (Tyr 51, Tyr134, Tyr 136, and Tyr 138) are also visible. Although a limited number of residues contributed to the interaction with the monosaccharide GlnNAc(6S), it is reasonable to assume that the binding of oligo- and polysaccharides will require a more extensive interaction surface. Indeed, the lipid-binding module of actinoporins is composed of a cluster of aromatic residues accepting up to four lipid molecules before pore

formation, and a region rich in basic residues surrounding it [46], being suitable for the engagement of carbohydrates bearing negative charges like GAGs [47, 48] (Figure S2).

Competition assay.

Taking advantage of the specific interaction of FraC with SEC columns like Superdex 200 10/300, we sought to elucidate if fragments of lipids could compete with the column for the toxin (Figure 5). As shown in Figure 5a, the elution of FraC (26.9 ml) occurs at a significantly higher volume than the total volume of the column (21.2 ml) because FraC binds reversibly to the resin of the column, composed of dextrans and agarose. The expected elution volume estimated from the molecular weight of the protein in the absence of interactions with the resin is 17.2 ml. If lipid- and sugar-binding sites were overlapping, lipids would competitively inhibit the binding of FraC to the column, thus reducing the volume at which the elution would take place. We employed phosphocholine (POC) as a water-soluble competitive inhibitor, since POC represents the headgroup of two major phospholipid molecules like phosphatidylcholine and sphygomyelin, to which FraC binds in liposomes [19, 26, 27].

As the concentration of POC in the equilibration buffer increased, the elution volume of FraC

(V) decreased (Figure 5b). A linear correlation between the concentration of POC and the inverse of the mobility $(V\text{-}V_{non})^{-1}$ is observed, as it would be expected for a phenomenon of competitive inhibition [40] (Figure 5c). The fit with equation (1) plot yields a straight line with a good correlation coefficient ($R^2 = 0.986$), corroborating the idea that the matrix of the column and POC are binding competitively to FraC.

The elution position of the mutein W112R/W116F, lacking binding to liposomes, appears at 19.2 ml, very close to the expected value for the non-interacting protein (17.2), and thus demonstrating that this mutein has a decreased ability to interact with the column. The residues Trp112 and Trp116 belonging to the attachment site for lipids 2 and 3 are in the vicinity of GlcNAc(6S), although we note that they are no completely adjacent (Figure S2). This observation suggest that the carbohydrate binding module also comprises an extended surface that could facilitate the engagement of oligo- and polysaccharides by the incremental and favorable interactions of multiple residues with multiple hexose rings. These results thus reinforced the notion that the carbohydrate- and lipid-binding modules consist of overlapping regions of FraC.

Structural similarity of FraC with fungal lectins.

The top structures ranked by structural similarity to FraC as obtained by the Dali server [49] are shown in Table S1. In addition to its close actinoporin relatives, FraC shows high structural homology with a variety of proteins from mushrooms, most of them lectins but also including the PFT pleurotolysin A, an two other PFT from bacteria. The similarities between actinoporins and and fungal lectins was already noted in previous studies [2, 17, 46, 50], but not until now it has been shown that both families of proteins shared the characteristic of binding carbohydrates. For example, both FraC and *Boletus edulis* lectin (BEL) display a core β-sandwich motif of quite similar topology (Figure S3). The β-sandwich of FraC is flanked by helices from both sides, whereas BEL display alpha-helices only one side of the β-sandwich. Importantly, the carbohydrate-binding site of FraC as observed in the crystal structure and the primary carbohydrate-binding site of BEL are in the same region between the β-sandwich and a helix (α2) (Figure 6), suggesting common evolutionary traits.

DISCUSSION

Herein, we have shown direct evidence that FraC of the family of actinoporins interact with glycans using structural regions that overlap with the lipid-binding module. The efficient use of

the interaction surface is therefore critical to recognize multiple receptors by a single-domain small protein. In contrast to FraC, large PFTs (> 40 kDa) often employ specialized domains to recognize multiple receptors on cell membranes [15]. Recently, it has been reported that some medium-sized PFTs (20-40 kDa) also have the ability to recognize multiple receptors [51]. However, the exact location of these receptor-binding sites has not been yet reported. Further research on this class of secondary binding sites in PFTs will shed light on the different strategies of recognition employed by toxins of different sizes and architectures. The ability of actinoporins to interact with carbohydrates is mirrored by the structurally homolog class of lectins from fungi (Figure 6).

Utilization of lipid-binding pockets as weak interaction spots for glycans might be a strategy shared by other PFTs. Indeed, the type of residues that contribute to the engagement of lipids and carbohydrates like those shown in Figure 4 appear often in both types of binding sites. First, aromatic residues are often observed at the recognition sites of lipids and glycans [47], and second, positively charged residues preferentially participate to attract the negatively charged GAGs and the headgroups of phospholipids [48]. Hydrogen bonds, considered a critical feature of glycan recognition [52] and binding to FraC (Figure 4), is also an important aspect for the

activity of actinoporins at the membrane level [19, 53, 54], thus reflecting an additional mechanistic similarity for the recognition of lipids and glycans by actinoporins in addition to aromatic interactions and electrostatic forces. In agreement with the idea of dual recognition sites, recent computational prediction of carbohydrate binding sites for cholesterol-dependent cytolysins suggested that they could engage glycans using the lipid-binding regions [7].

The quantitative analysis indicated that the interaction of FraC with saccharides ($K_D \approx 10^{-5}$ M) is significantly weaker than that of lipidic membranes ($K_D \approx 10^{-7}$ M). Moreover, the dissociation rate constant of FraC-glycan interaction is fast ($k_{off} \approx 10^{0}$ s^{-1}) compared with the nearly irreversible interaction of FraC (and the close homolog equinatoxin II) with liposomes [18, 55]. This analysis suggests that FraC and glycans form transient complexes of short lifetime, helping to accumulate the toxin near on glycan-rich surfaces, but without compromising its ability to interact with membrane lipids. Notably, the mucus layer of fishes contains significant amounts of GAGs [56, 57], that could act as a concentration platform for the accumulation of actinoporins on the surface of target preys. Further research to ascertain the exact glycan composition of mucus of the fish skin and the ability of FraC to accommodate there will be necessary to prove the full biological significance of this mechanism. In part, the failure of the glycan screen to find more

specific and high-affinity glycans could be explained because this array employs only mammalian glycans, which are not among natural targets of sea anemones. Although the biological function of the carbohydrate-actinoporin interaction has not been fully established in our study, the recruitment of actinoporins on the surface of target cells and/or tissues by low affinity interaction with carbohydrates could be an effective strategy to enhance their activity in conditions of high dilution such as the marine environment.

In summary, our data showed that FraC utilize the glycans to enhance its hemolytic activity. FraC binds to saccharides without particular specificity but and it is enhanced by negative charged on the glycan. Notably, residues interacting with the carbohydrates also belong to the phospholipid binding module of the toxin. This dual usage of residues is an economic strategy that FraC may employ to achieve binding of multiple ligands with its limited molecular size.

Acknowledgments.

This work was supported by JSPS Grants-in-Aid for Scientific Research 25249115 (K. Tsumoto) and 15K06962 (J.M.M.C.), and a Grant-in-Aid for JSPS fellows (K. Tanaka). We thank the staff of the Photon Factory (Tsukuba, Japan) for excellent technical support. Access to beamline

AR-NE3A was granted by the Photon Factory Advisory Committee (Proposal Number 2013G738). We acknowledge the Protein-glycan Interaction Resource at the Consortium for Functional Glycomics (Grant R24 GM098791) for the glycan screening. We thank Prof. Juan Manuel González-Mañas for valuable advice.

Accession number

The coordinates and structure factors for the structures of FraC in complex with GlcNAc(6S) have been deposited in the PDB under accession code 5GWF.

Supplemental Information.

Supplemental Information includes one table and three figures.

Author contributions.

K. Tanaka, J.M.M.C., and K. Tsumoto designed research. K. Tanaka performed experiments of hemolysis, crystallization, chromatography, SPR, protein labeling, and site-directed mutagenesis. K.M. performed experiments of hemolysis. J.M.M.C. performed crystallization experiments, and processed and determined the crystal structure. All authors discussed the results. K. Tanaka and J.M.M.C. wrote the manuscript, and received approval from K.M. and K. Tsumoto.

Competing interest statement.

The authors declare no competing financial interest.

REFERENCES

[1] Iacovache, I., Bischofberger, M. & van der Goot, F. G. 2010 Structure and assembly of pore-forming proteins. *Curr. Opin. Struct. Biol.* **20**, 241-246. (DOI:10.1016/j.sbi.2010.01.013).

[2] Anderluh, G. & Lakey, J. H. 2008 Disparate proteins use similar architectures to damage membranes. *Trends Biochem. Sci.* **33**, 482-490. (DOI:10.1016/J.Tibs.2008.07.004).

[3] Gilbert, R. J. C., Serra, M. D., Froelich, C. J., Wallace, M. I. & Anderluh, G. 2014 Membrane pore formation at protein-lipid interfaces. *Trends Biochem. Sci.* **39**, 510-516. (DOI:10.1016/j.tibs.2014.09.002).

[4] Baran, K., Dunstone, M., Chia, J., Ciccone, A., Browne, K. A., Clarke, C. J. P., Lukoyanova, N., Saibil, H., Whisstock, J. C., Voskoboinik, I., et al. 2009 The molecular basis for perforin oligomerization and transmembrane pore assembly. *Immunity* **30**, 684-695. (DOI:10.1016/j.immuni.2009.03.016).

[5] Serna, M., Giles, J. L., Morgan, B. P. & Bubeck, D. 2016 Structural basis of complement membrane attack complex formation. *Nat. Commun.* **7**. (DOI:10.1038/Ncomms10587).

[6] Tilley, S. J. & Saibil, H. R. 2006 The mechanism of pore formation by bacterial toxins. *Curr.*

Opin. Struct. Biol. **16**, 230-236. (DOI:10.1016/j.sbi.2006.03.008).

[7] Shewell, L. K., Harvey, R. M., Higgins, M. A., Day, C. J., Hartley-Tassell, L. E., Chen, A. Y., Gillen, C. M., James, D. B. A., Alonzo, F., Torres, V. J., et al. 2014 The cholesterol-dependent cytolysins pneumolysin and streptolysin O require binding to red blood cell glycans for hemolytic activity. *Proc. Natl. Acad. Sci. USA* **111**, E5312-E5320. (DOI:10.1073/pnas.1412703111).

[8] Farrand, S., Hotze, E., Friese, P., Hollingshead, S. K., Smith, D. F., Cummings, R. D., Dale, G. L. & Tweten, R. K. 2008 Characterization of a streptococcal cholesterol-dependent cytolysin with a Lewis y and b specific lectin domain. *Biochemistry* **47**, 7097-7107. (DOI:10.1021/bi8005835).

[9] Feil, S. C., Lawrence, S., Mulhern, T. D., Holien, J. K., Hotze, E. M., Farrand, S., Tweten, R. K. & Parker, M. W. 2012 Structure of the lectin regulatory domain of the cholesterol-dependent cytolysin lectinolysin reveals the basis for its lewis antigen specificity. *Structure* **20**, 248-258. (DOI:10.1016/j.str.2011.11.017).

[10] Bouyain, S. & Geisbrechtz, B. V. 2012 Host glycan recognition by a pore forming toxin. *Structure* **20**, 197-198. (DOI:10.1016/j.str.2012.01.013).

[11] De, S., Bubnys, A., Alonzo, F., Hyun, J., Lary, J. W., Cole, J. L., Torres, V. J. & Olson, R.

2015 The relationship between glycan binding and direct membrane interactions in *Vibrio cholerae* cytolysin, a channel-forming toxin. *J. Biol. Chem.* **290**, 28402-28415. (DOI:10.1074/jbc.M115.675967).

[12] Levan, S., De, S. & Olson, R. 2013 *Vibrio cholerae* cytolysin recognizes the heptasaccharide core of complex N-glycans with nanomolar affinity. *J. Mol. Biol.* **425**, 944-957. (DOI:10.1016/j.jmb.2012.12.016).

[13] Turnbull, W. B., Precious, B. L. & Homans, S. W. 2004 Dissecting the cholera toxin-ganglioside GM1 interaction by isothermal titration calorimetry. *J. Am. Chem. Soc.* **126**, 1047-1054. (DOI:10.1021/ja0378207).

[14] Abrami, L., Fivaz, M. & van der Goot, F. G. 2000 Adventures of a pore-forming toxin at the target cell surface. *Trends Microbiol.* **8**, 168-172. (DOI:10.1016/S0966-842x(00)01722-4).

[15] Dal Peraro, M. & van der Goot, F. G. 2016 Pore-forming toxins: ancient, but never really out of fashion. *Nat. Rev. Microbiol.* **14**, 77-92. (DOI:10.1038/nrmicro.2015.3).

[16] Iacovache, I., van der Goot, F. G. & Pernot, L. 2008 Pore formation: an ancient yet complex form of attack. *Biochim. Biophys. Acta* **1778**, 1611-1623. (DOI:10.1016/j.bbamem.2008.01.026).

[17] Kristan, K. C., Viero, G., Dalla Serra, M., Macek, P. & Anderluh, G. 2009 Molecular

mechanism of pore formation by actinoporins. *Toxicon* **54**, 1125-1134. (DOI:10.1016/j.toxicon.2009.02.026).

[18] Bakrac, B., Gutiérrez-Aguirre, I., Podlesek, Z., Sonnen, A. F., Gilbert, R. J., Macek, P., Lakey, J. H. & Anderluh, G. 2008 Molecular determinants of sphingomyelin specificity of a eukaryotic pore-forming toxin. *J. Biol. Chem.* **283**, 18665-18677. (DOI:10.1074/jbc.M708747200).

[19] Tanaka, K., Caaveiro, J. M. M., Morante, K., Gonzalez-Manas, J. M. & Tsumoto, K. 2015 Structural basis for self-assembly of a cytolytic pore lined by protein and lipid. *Nat. Commun.* **6**, 6337. (DOI:DOI 10.1038/ncomms7337).

[20] Barlic, A., Gutiérrez-Aguirre, I., Caaveiro, J. M. M., Cruz, A., Ruíz-Arguello, M. B., Pérez-Gil, J. & González-Mañas, J. M. 2004 Lipid phase coexistence favors membrane insertion of equinatoxin-II, a pore-forming toxin from *Actinia equina*. *J. Biol. Chem.* **279**, 34209-34216. (DOI:10.1074/jbc.M313817200).

[21] Schön, P., García-Sáez, A. J., Malovrh, P., Bacia, K., Anderluh, G. & Schwille, P. 2008 Equinatoxin II permeabilizing activity depends on the presence of sphingomyelin and lipid phase coexistence. *Biophys. J.* **95**, 691-698. (DOI:10.1529/biophysj.108.129981).

[22] Caaveiro, J. M. M., Echabe, I., Gutierrez-Aguirre, I., Nieva, J. L., Arrondo, J. L. R. & Gonzalez-Manas, J. M. 2001 Differential interaction of equinatoxin II with model membranes in response to lipid composition. *Biophys. J.* **80**, 1343-1353.

[23] Athanasiadis, A., Anderluh, G., Maček, P. & Turk, D. 2001 Crystal structure of the soluble form of equinatoxin II, a pore-forming toxin from the sea anemone *Actinia equina*. *Structure* **9**, 341-346. (DOI:10.1016/S0969-2126(01)00592-5).

[24] Mancheño, J. M., Martín-Benito, J., Martínez-Ripoll, M., Gavilanes, J. G. & Hermoso, J. A. 2003 Crystal and electron microscopy structures of sticholysin II actinoporin reveal insights into the mechanism of membrane pore formation. *Structure* **11**, 1319-1328. (DOI:10.1016/j.str.2003.09.019).

[25] Mechaly, A. E., Bellomio, A., Gil-Cartón, D., Morante, K., Valle, M., González-Mañas, J. M. & Guerin, D. M. A. 2011 Structural insights into the oligomerization and architecture of eukaryotic membrane pore-forming toxins. *Structure* **19**, 181-191. (DOI:10.1016/j.str.2010.11.013).

[26] Morante, K., Caaveiro, J. M. M., Tanaka, K., Gonzalez-Manas, J. M. & Tsumoto, K. 2015 A pore-forming toxin requires a specific residue for its activity in membranes with particular

physicochemical properties. *J. Biol. Chem.* **290**, 10850-10861. (DOI:10.1074/jbc.M114.615211).

[27] Morante, K., Bellomio, A., Gil-Carton, D., Redondo-Morata, L., Sot, J., Scheuring, S., Valle, M., Gonzalez-Manas, J. M., Tsumoto, K. & Caaveiro, J. M. 2016 Identification of a membrane-bound prepore species clarifies the lytic mechanism of actinoporins. *J. Biol. Chem.* **291**, 19210-19219. (DOI:10.1074/jbc.M116.734053).

[28] Alegre-Cebollada, J., Cunietti, M., Herrero-Galán, E., Gavilanes, J. G. & Martínez-del-Pozo, Á. 2008 Calorimetric scrutiny of lipid binding by sticholysin II toxin mutants. *J. Mol. Biol.* **382**, 920-930. (DOI:10.1016/j.jmb.2008.07.053).

[29] Rojko, N., Dalla Serra, M., Macek, P. & Anderluh, G. 2016 Pore formation by actinoporins, cytolysins from sea anemones. *Biochim. Biophys. Acta* **1858**, 446-456. (DOI:10.1016/j.bbamem.2015.09.007).

[30] Wloka, C., Mutter, N. L., Soskine, M. & Maglia, G. 2016 Alpha-helical fragaceatoxin C nanopore engineered for double-stranded and single-stranded nucleic acid analysis. *Angew. Chem. Int. Ed. Engl.* **55**, 12494-12498. (DOI:10.1002/anie.201606742).

[31] Bellomio, A., Morante, K., Barlic, A., Gutiérrez-Aguirre, I., Viguera, A. R. & González-Mañas, J. M. 2009 Purification, cloning and characterization of fragaceatoxin C, a

novel actinoporin from the sea anemone *Actinia fragacea*. *Toxicon* **54**, 869-880. (DOI:10.1016/j.toxicon.2009.06.022).

[32] de los Rios, V., Mancheno, J. M., del Pozo, A. M., Alfonso, C., Rivas, G., Onaderra, M. & Gavilanes, J. G. 1999 Sticholysin II, a cytolysin from the sea anemone *Stichodactyla helianthus*, is a monomer-tetramer associating protein. *FEBS Lett.* **455**, 27-30. (DOI:10.1016/S0014-5793(99)00846-7).

[33] Morante, K., Caaveiro, J. M. M., Viguera, A. R., Tsumoto, K. & Gonzalez-Manas, J. M. 2015 Functional characterization of Val60, a key residue involved in the membrane-oligomerization of fragaceatoxin C, an actinoporin from Actinia fragacea. *FEBS Lett.* **589**, 1840-1846. (DOI:10.1016/j.febslet.2015.06.012).

[34] Ito, M., Ikegami, Y. & Yamagata, T. 1991 Activator proteins for glycosphingolipid hydrolysis by endoglycoceramidases - elucidation of biological functions of cell-surface glycosphingolipids *in situ* by endoglycoceramidases made possible using these activator proteins. *J. Biol. Chem.* **266**, 7919-7926.

[35] Drickamer, K. & Taylor, M. E. 2002 Glycan arrays for functional glycomics. *Genome Biol.* **3**, 1-4.

[36] McCoy, A. J., Grosse-Kunstleve, R. W., Adams, P. D., Winn, M. D., Storoni, L. C. & Read, R. J. 2007 *Phaser* crystallographic software. *J. Appl. Crystallogr.* **40**, 658-674. (DOI:10.1107/S0021889807021206).

[37] Murshudov, G. N., Vagin, A. A. & Dodson, E. J. 1997 Refinement of macromolecular structures by the maximum-likelihood method. *Acta Crystallogr. D Struct. Biol.* **53**, 240-255. (DOI:10.1107/S0907444996012255).

[38] Emsley, P., Lohkamp, B., Scott, W. G. & Cowtan, K. 2010 Features and development of Coot. *Acta Crystallogr. D Struct. Biol.* **66**, 486-501. (DOI:10.1107/S0907444910007493).

[39] Laskowski, R. A., Macarthur, M. W., Moss, D. S. & Thornton, J. M. 1993 *PROCHECK*: a program to check the stereochemical quality of protein structures. *J. Appl. Crystallogr.* **26**, 283-291. (DOI:10.1107/S0021889892009944).

[40] Dunn, B. M. & Chaiken, I. M. 1974 Quantitative affinity chromatography - determination of binding constants by elution with competitive inhibitors. *Proc. Natl. Acad. Sci. USA* **71**, 2382-2385. (DOI:10.1073/Pnas.71.6.2382).

[41] Alm, I., Garcia-Linares, S., Gavilanes, J. G., Martinez-del-Pozo, A. & Slotte, J. P. 2015 Cholesterol stimulates and ceramide inhibits Sticholysin II-induced pore formation in complex

bilayer membranes. *Biochim. Biophys. Acta* **1848**, 925-931.

(DOI:10.1016/j.bbamem.2014.12.017).

[42] Bernheimer, A. W. & Avigad, L. S. 1976 Properties of a toxin from sea-anemone Stoichactis helianthus, including specific binding to sphingomyelin. *Proc. Natl. Acad. Sci. USA* **73**, 467-471. (DOI:10.1073/Pnas.73.2.467).

[43] Tejuca, M., Dalla Serra, M., Potrich, C., Alvarez, C. & Menestrina, G. 2001 Sizing the radius of the pore formed in erythrocytes and lipid vesicles by the toxin sticholysin I from the sea anemone Stichodactyla helianthus. *J. Membr. Biol.* **183**, 125-135. (DOI:10.1007/S00232-001-0060-Y).

[44] Belmonte, G., Pederzolli, C., Macek, P. & Menestrina, G. 1993 Pore formation by the sea-anemone cytolysin equinatoxin-Ii in red-blood-cells and model lipid-membranes. *J. Membr. Biol.* **131**, 11-22. (DOI:10.1007/Bf02258530).

[45] Kobe, A., Caaveiro, J. M. M., Tashiro, S., Kajihara, D., Kikkawa, M., Mitani, T. & Tsumoto, K. 2013 Incorporation of rapid thermodynamic data in fragment-based drug discovery. *J. Med. Chem.* **56**, 2155-2159. (DOI:10.1021/jm301603n).

[46] García-Ortega, L., Alegre-Cebollada, J., García-Linares, S., Bruix, M., Martínez-del-Pozo, A.

& Gavilanes, J. G. 2011 The behavior of sea anemone actinoporins at the water-membrane interface. *Biochim. Biophys. Acta* **1808**, 2275-2288. (DOI:10.1016/j.bbamem.2011.05.012).

[47] Asensio, J. L., Arda, A., Canada, F. J. & Jimenez-Barbero, J. 2013 Carbohydrate-aromatic interactions. *Acc. Chem. Res.* **46**, 946-954. (DOI:10.1021/ar300024d).

[48] Esko, J. D. & Linhardt, R. J. 2009 Proteins that bind sulfated glycosaminoglycans. In *Essentials of glycobiology* (eds. A. Varki, R. D. Cummings, J. D. Esko, H. H. Freeze, P. Stanley, C. R. Bertozzi, G. W. Hart & M. E. Etzler), 2nd ed. Cold Spring Harbor (NY).

[49] Holm, L. & Rosenstrom, P. 2010 Dali server: conservation mapping in 3D. *Nucleic Acids Res.* **38**, W545-W549. (DOI:10.1093/nar/gkq366).

[50] Gutierrez-Aguirre, I., Trontelj, P., Macek, P., Lakey, J. H. & Anderluh, G. 2006 Membrane binding of zebrafish actinoporin-like protein: AF domains, a novel superfamily of cell membrane binding domains. *Biochem. J.* **398**, 381-392. (DOI:10.1042/BJ20060206).

[51] DuMont, A. L. & Torres, V. J. 2014 Cell targeting by the *Staphylococcus aureus* pore-forming toxins: it's not just about lipids. *Trends Microbiol.* **22**, 21-27. (DOI:10.1016/j.tim.2013.10.004).

[52] Weis, W. I. & Drickamer, K. 1996 Structural basis of lectin-carbohydrate recognition. *Annu.*

Rev. Biochem. **65**, 441-473.

[53] Garcia-Linares, S., Palacios-Ortega, J., Yasuda, T., Astrand, M., Gavilanes, J. G., Martinez-del-Pozo, A. & Slotte, J. P. 2016 Toxin-induced pore formation is hindered by intermolecular hydrogen bonding in sphingomyelin bilayers. *Biochim. Biophys. Acta* **1858**, 1189-1195. (DOI:10.1016/j.bbamem.2016.03.013).

[54] Maula, T., Isaksson, Y. J. E., Garcia-Linares, S., Niinivehmas, S., Pentikainen, O. T., Kurita, M., Yamaguchi, S., Yamamoto, T., Katsumura, S., Gavilanes, J. G., et al. 2013 2NH and 3OH are crucial structural requirements in sphingomyelin for sticholysin II binding and pore formation in bilayer membranes. *Biochim. Biophys. Acta* **1828**, 1390-1395. (DOI:10.1016/j.bbamem.2013.01.018).

[55] Tanaka, K., Caaveiro, J. M. M. & Tsumoto, K. 2015 Bidirectional transformation of a metamorphic protein between the water-soluble and transmembrane native states. *Biochemistry* **54**, 6863-6866. (DOI:10.1021/acs.biochem.5b01112).

[56] Shephard, K. L. 1994 Functions for Fish Mucus. *Rev. Fish Biol. Fish.* **4**, 401-429. (DOI:10.1007/Bf00042888).

[57] Vandewinkel, J. G. J., Vankuppevelt, T. H. M. S. M., Janssen, H. M. J. & Lock, R. A. C.

1986 Glycosaminoglycans in the skin mucus of rainbow-trout (Salmo-Gairdneri). *Comp. Biochem. Physiol. B Biochem. Mol. Biol.* **85**, 473-475. (DOI:10.1016/0305-0491(86)90030-1).

Table 1: Data collection and refinement statistics.

Statistical values given in parenthesis refer to the highest resolution bin.

Data Collection	**FraC + GlcNAc(6S)**
Space Group	P 1 2_1 1
Unit cell	
a, b, c, Å	77.16, 44.40, 114.36
α, β, γ, °	90.0, 92.76, 90.0
Resolution, Å	37.1 – 1.55 (1.63 – 1.55)
Wavelength, Å	1.000
Observations	543,367 (59,662)
Unique reflections	103,405 (12,516)
$R_{merge.}$ (%)[a]	0.069 (0.293)
CC(1/2)	0.997 (0.937)
$I / \sigma (I)$	14.8 (4.5)
Multiplicity	5.3 (5.4)
Completeness (%)	91.8 (76.8)
Refinement Statistics	
Resolution, Å	37.1 – 1.55
R_{work} / R_{free}, %[b]	11.8 / 16.3 (13.4 / 17.3)
No. atoms	6,526
No. protein chains	4
No. protein residues	708
No. sugar molecules	2
No. waters molecules	775
No. other (not solvent)	15
Protein B-factor, $Å^2$	15.2
Sugar B-factor, $Å^2$	23.3
Water B-factor, $Å^2$	25.9
Other B-factor (not solvent), $Å^2$	22.3
Ramachandran Plot	
Preferred Regions, %	89.4
Allowed Regions, %	10.6
Outliers (%)	0
RMSD bond, Å	0.012
RMSD angle, °	1.5
PDB identification code	5GWF

[a] $R_{merge} = \Sigma_{hkl} \Sigma_i |(I(hkl)_i - [I(hkl)]| / \Sigma_{hkl} \Sigma_i I(hkl)$.

[b] $R_{work} = \Sigma_{hkl} |F(hkl)_o - [F(hkl)_c]| / \Sigma_{hkl} F(hkl)_o$; R_{free} was calculated as R_{work}, where $F(hkl)_o$ values were taken from 3% of data not included in the refinement.

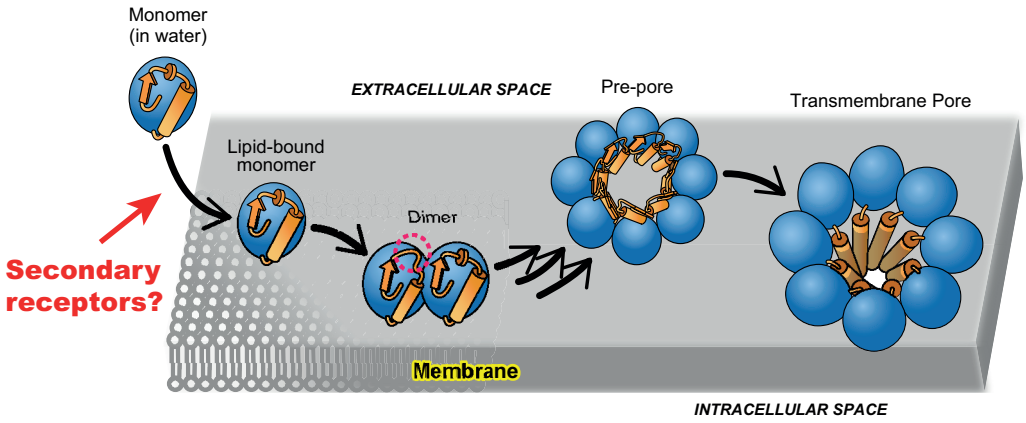

Figure 1. Mechanism of actinoporins. In this study we will address the hypothesis that carbohydrates act as weak secondary receptors, possibly helping to concentrate actinoporins on the surface of target cells. The dashed red circle represents a conformational change at the N-terminal region upon dimerization [19]. The existence of a prepore species bound to membranes was recently visualized [27]. The figure was adapted from Tanaka *et al* [19].

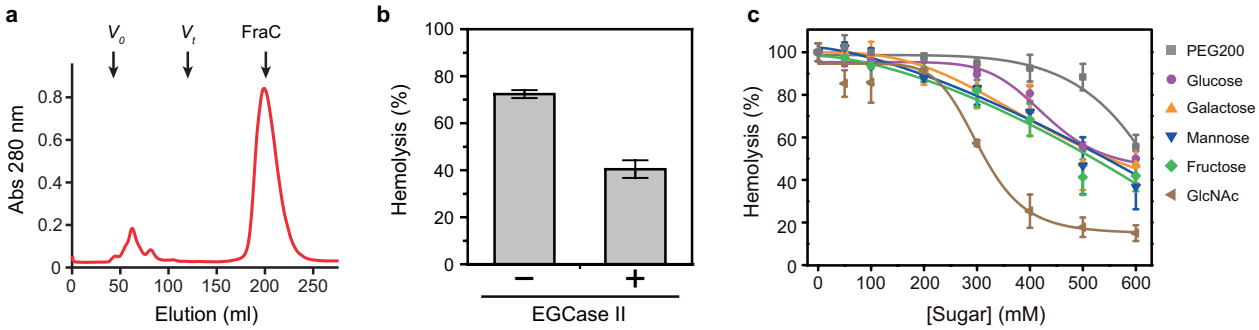

Figure 2. Evidence of the interaction between FraC and carbohydrates. (a) Delayed elution profile of FraC on a column of SEC (HiLoad 16/600 Superdex 75) consisting of a composite base matrix of dextran and agarose. Anomalous elution profiles are also observed in other carbohydrate-based gel-filtration columns. V_0, V_t and FraC indicate the void volume (45 ml), the column volume (120 ml), and the elution of the monomeric water-soluble form of FraC (198 ml), respectively. **(b)** Hemolysis of RBC treated with EGCase II, or untreated, in the presence of 19.5 nM FraC. The values corresponding to 100% and 0% hemolysis were obtained by addition of Triton X-100 (1% v:v) or buffer. **(c)** Inhibitory effect of monosaccharides on hemolysis. The protein was added at a final concentration of 25 µM. The compounds employed were PEG-200 (gray) and monosaccharides glucose (magenta), galactose (orange), mannose (blue), fructose (green), and GlcNAc (light brown).

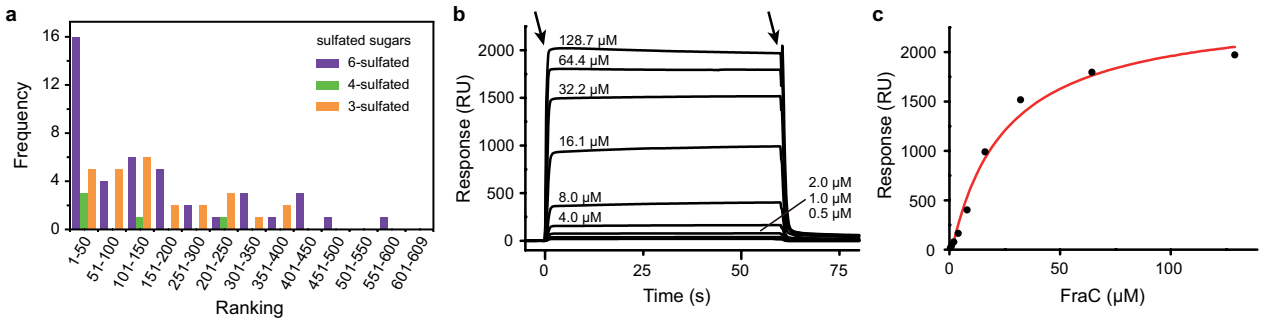

Figure 3. Glycan screening and binding analysis by SPR. (a) The region corresponding to the top hits on a binding screen with 609 different glycans attached on a microarray is enriched on sulfated oligosaccharides. The sulfated glycans were classified according to the position of the sulfate group. Position 6, position 4, and position 3 are indicated by the purple, green and orange bars, respectively. **(b)** Kinetics of interaction between FraC and chondroitin sulfate C determined by SPR. The chondroitin sulfate C was immobilized on a chip and FraC was flowed at 0.5, 1.0, 2.0, 4.0, 8.0, 16.1, 32.2, 64.4 and 128.7 µM. The first and second arrow indicates the interval when FraC is accessing the sensor-chip where the polysaccharide is immobilized. Data were fit to single-site model to calculate kinetic parameters. **(c)** Determination of the equilibrium constant from the binding response in equilibrium (K_D = 24 µM).

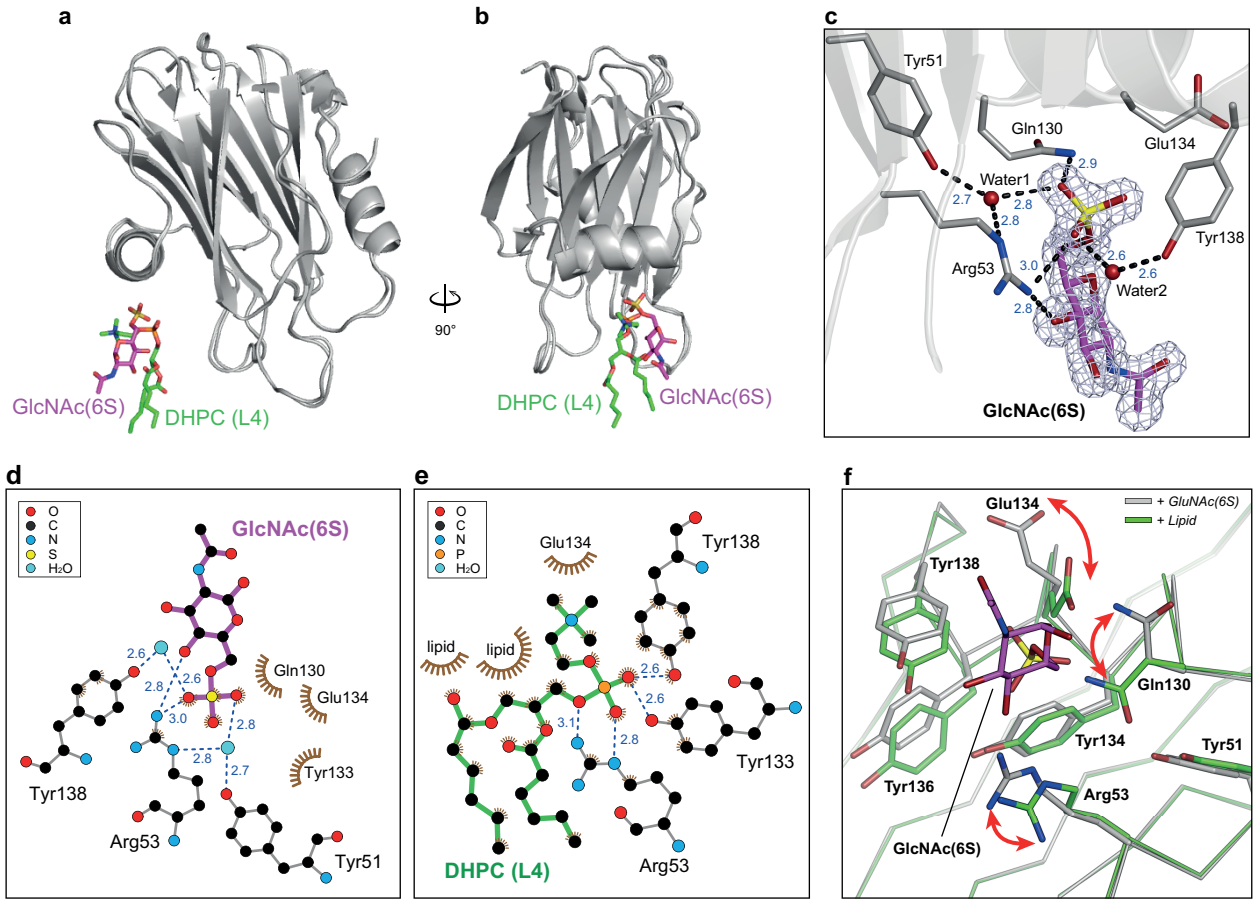

Figure 4. High-resolution crystal structure of FraC in complex with GlcNAc(6S). **(a, b)** Comparison of the crystal structure of Frac with GlcNAc(6S) (this work) or lipids (PDB entry code 4TQS) bound. The position of GlcNAc(6S) (magenta) and DHPC (green) overlap. **(c)** Close up view of the monosaccharide bound to FraC. The mesh corresponds to the sigma-A weighted 2Fo – Fc electron density map (σ = 1.0) of GlcNAc(6S). GlcNAc(6S) is shown in magenta. Protein-sugar and water mediated hydrogen bonds are depicted with dashed lines, and their corresponding distances indicated in blue. **(d, e)** Residue environments around GlcNAc(6s) (panel d) and DHPC L4 (panel e) as calculated with the program LigPlot^{+}. **(f)** Conformational change in residues of the binding pocket in response to the presence of lipid (green) or carbohydrate (gray). GlcNAc(6S) is depicted in magenta. For clarity purposes the lipid has been omitted form the figure. The arrows indicate the movement of the residues experiencing the greatest conformational changes.

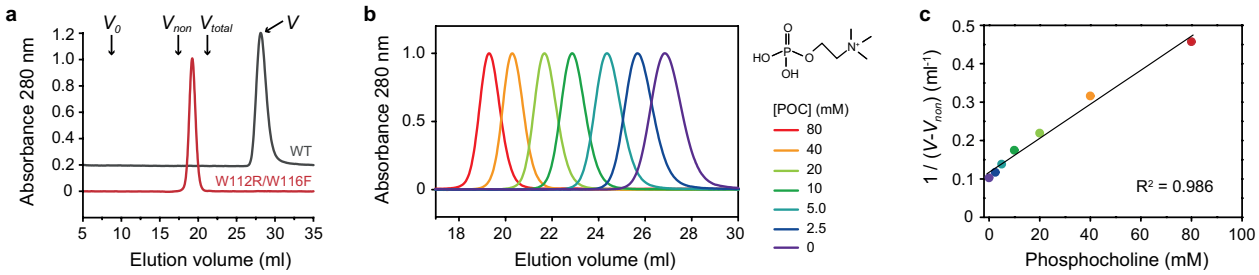

Figure 5. Elution profile of FraC on a Superdex column. (a) Chromatographic profile of WT FraC (black line) and mutein W112R/W116F (red line). The arrows point at the position of the void volume (V_0), the volume of FraC in the absence of interactions (V_{non}), the total volume (V_{total}) and the elution volume of FraC (V) as given in equation (1). **(b)** SEC profile of FraC in the presence of increasing amounts of POC (0, 2.5, 5, 10, 20, 40 and 80 mM). **(c)** Plot of 1 / (V-V_{non}) as a function of the concentration of POC. The black line corresponds to the fitted line from equation (1). The regression coefficient is also given in the figure (R^2 = 0.986).

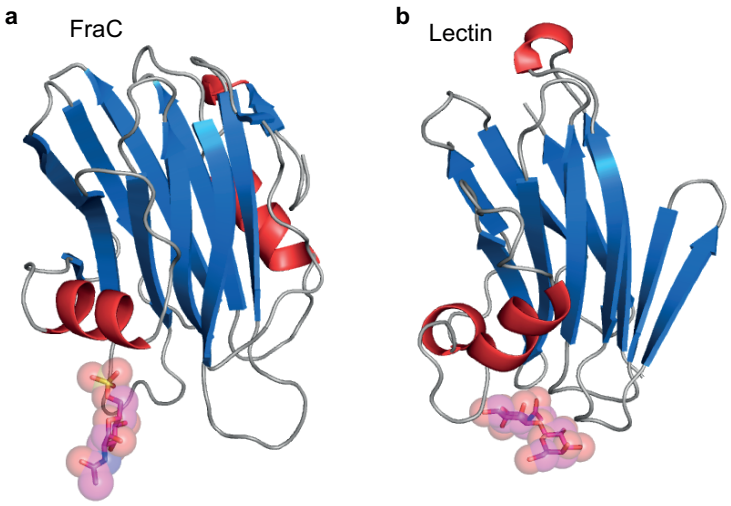

Figure 6. Structural comparison of FraC with a fungal lectin. Location of a carbohydrate bound to **(a)** FraC and **(b)** to the lectin from *Boletus edulis* (PDB ID: 3QDX). The carbohydrate bound to FraC is the monosaccharide GlcNAc(6S), whereas the carbohydrate bound to the lectin is di-GlcNAc.

Supplementary Information

Hemolytic actinoporins interact with carbohydrates using their lipid-binding module.

Koji Tanaka[1], Jose M.M. Caaveiro[2,*], Koldo Morante[2], and Kouhei Tsumoto[1,2,3,*]

[1]Department of Chemistry and Biotechnology, School of Engineering, The University of Tokyo, Bunkyo-ku, Tokyo 113-8656, Japan, [2]Department of Bioengineering, School of Engineering, The University of Tokyo, Bunkyo-ku, Tokyo, 113-8656, Japan, [3]The Institute of Medical Science, The University of Tokyo, Minato-ku, Tokyo, 108-8639, Japan.

Corresponding author: JMMC, Email jose@protein.t.u-tokyo.ac.jp

Corresponding author: KT, Email tsumoto@bioeng.t.u-tokyo.ac.jp

Footnote.

Current address of JMMC: Graduate School of Pharmaceutical Sciences, Kyushu University, 3-1-1 Maidashi, Higashi-ku, Fukuoka, 812-8582, Japan.

Table S1. Structural homology of FraC (http://ekhidna.biocenter.helsinki.fi/dali_server/start).

PDB ID	Protein	Class	Z score	RMSD	No. res.[a]	No. ali.[b]	%id[c]
3vwi	Fragaceatoxin C	PFT	38.2	0.2	177	177	100
1iaz	Equinatoxin II	PFT	35.4	0.4	175	174	90
1gwy	Sticholysin II	PFT	34.6	0.7	175	175	63
2ks4	Sticholysin I	PFT	22.5	2.0	176	172	61
4jox	Insecticidal protein cry34Ab1	PFT	14.3	1.5	118	112	18
4oeb	Pleurotolysin A	PFT	11.4	2.4	135	116	14
3qdx[d]	*Boletus edulis* lectin	Lectin	11.2	2.5	142	123	11
1x99	*Xerocomus chrysenteron* lectin	Lectin	11	2.7	143	125	13
2ofd[d]	*Sclerotium rolfsii* lectin	Lectin	10.9	2.7	141	124	11
3a57	Thermostable direct hemolysin	PFT	10.5	3.3	154	131	4
1y2v[d]	*Agaricus bisporus* lectin	Lectin	10.5	2.6	143	122	12

[a] Number of residues.

[b] Number of structurally equivalent residues.

[c] Percentage of identical amino acids among structurally equivalent residues.

[d] Structures with sugars found.

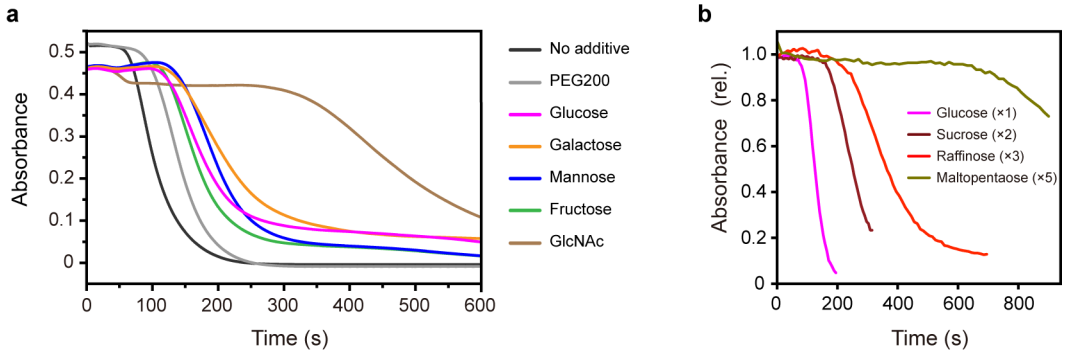

Figure S1. Kinetics of hemolysis by FraC in the presence of saccharides. (a) Inhibitory effect of various monosaccharides. The hemolytic toxin was added at a final concentration of 25 nM. The concentration of PEG200 (gray) and monosaccharides glucose (magenta), galactose (orange), mannose (blue), fructose (green), or GlcNAc (light brown) was 400 mM. **(b)** Influence of the number of hexoses of the saccharide on the kinetics of hemolysis. Data for glucose (one unit, magenta), sucrose (two units, brown), raffinose (three units, red) and maltopentaose (five units, olive) are shown.

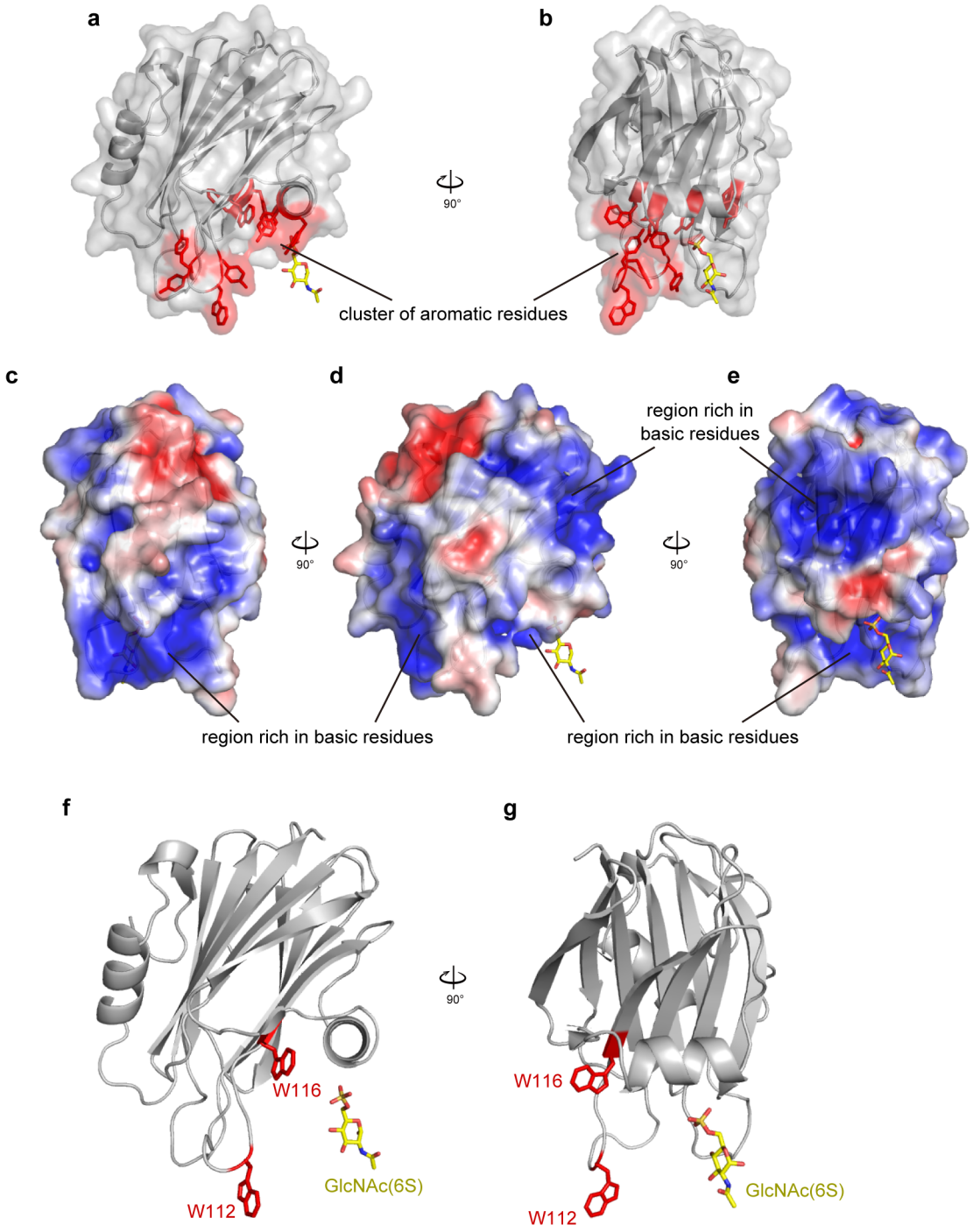

Figure S2. Depiction of the lipid/carbohydrate binding region of FraC. **(a, b)** The cluster of aromatic residues of FraC are colored in red. **(c-e)** Electrostatic potential of FraC. The color gradient set from red to blue represents negative (-3 kT/e) to positive (+3 kT/e) electrostatic potentials. **(f, g)** Location of residues W112 and W116 with respect to the sugar GlcNAc(6S).

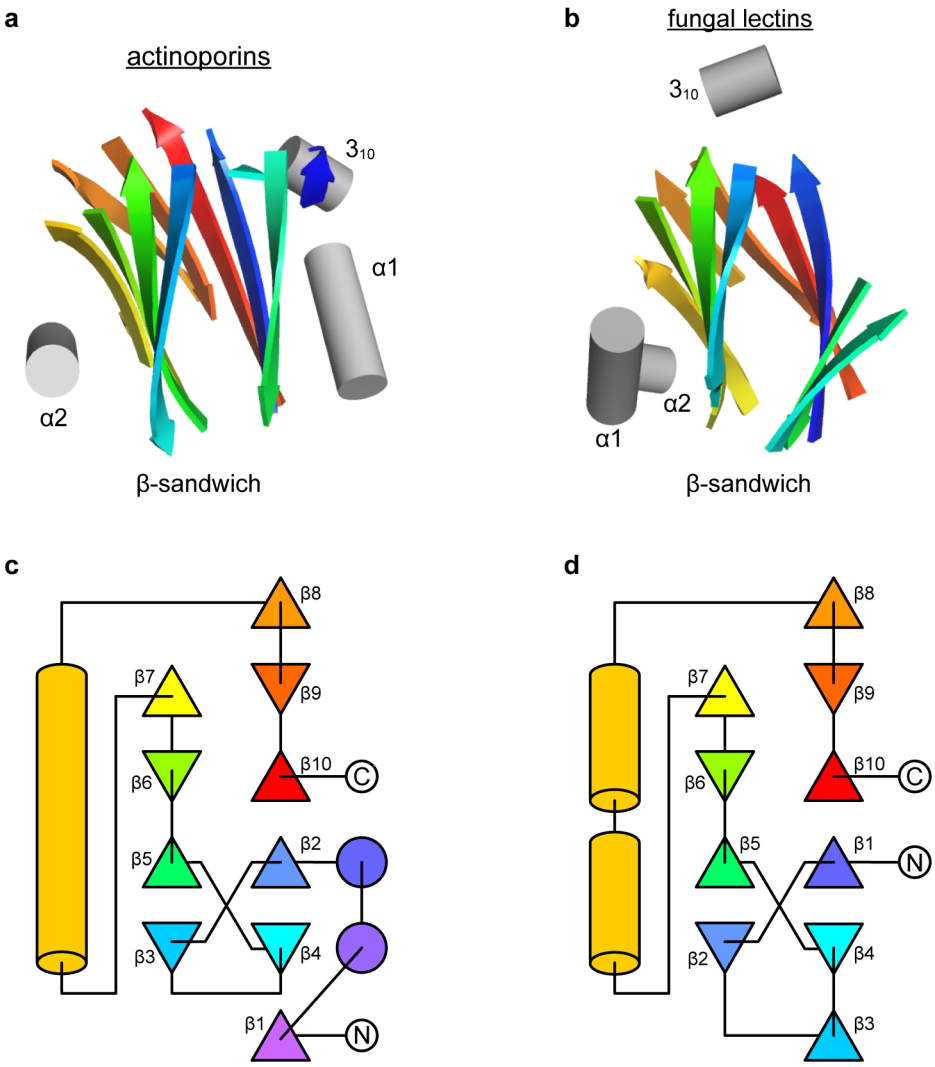

Figure S3. Comparison of FraC with a fungal lectin. (a, b) Side view of FraC (a) and a fungal lectin from *Boletus edulis* (b). Helices and β-strands are shown as cylinders and arrows, respectively. The β-strands are colored in rainbow from blue (near N-terminus) to red (near C-terminus). **(c, d)** Topology map of actinoporins (c) and the fungal lectin from *Boletus edulis* (d). Circles and cylinders represent helices. β-strands are shown as triangles that are numbered sequentially. Triangles drawn with opposite orientation indicate antiparallel strands.